JACS
JOURNAL OF THE AMERICAN CHEMICAL SOCIETY
Article
pubs.acs.org/JACS

Synthesis, Structures, and Photophysical Properties of π-Expanded Oligothiophene 8-mers and Their Saturn-Like C_{60} Complexes

Hideyuki Shimizu,[†] José D. Cojal González,[‡] Masashi Hasegawa,[§] Tohru Nishinaga,[†] Tahmina Haque,[†] Masayoshi Takase,[†] Hiroyuki Otani,[∥] Jürgen P. Rabe,[‡] and Masahiko Iyoda*[,†]

[†]Department of Chemistry, Graduate School of Science and Engineering, Tokyo Metropolitan University, Hachioji, Tokyo 192-0397, Japan

[‡]Department of Physics & IRIS Adlershof, Humboldt University Berlin, Newtonstrasse 15, 12489 Berlin, Germany

[§]Department of Chemistry, School of Science, Kitasato University, 1-15-1 Kitasato, Minami-ku, Sagamihara, Kanagawa 252-0373, Japan

[∥]Graduate School of Environment and Information Sciences, Yokohama National University, Hodogaya-ku, Yokohama, Kanagawa 240-8501, Japan

Supporting Information

ABSTRACT: Two isomers of a multifunctional π-expanded macrocyclic oligothiophene 8-mer, *E,E*-**1** and *Z,Z*-**1**, were synthesized using a McMurry coupling of a dialdehyde composed of four 2,5-thienylene and three ethynylene units under high dilution conditions. On the other hand, cyclo[8]-(2,5-thienylene-ethynylene) **2** was synthesized by intramolecular Sonogashira cyclization of ethynyl bromide **5**. From STM measurements, both *E,E*-**1** and *Z,Z*-**1** formed self-assembled monolayers at the solid−liquid interface to produce porous networks, and from X-ray analyses of *E,E*-**1** and **2**, both compounds had a round shape with a honeycomb stacked structure. *E,E*-**1** formed various fibrous polymorphs due to nanophase separation of the macrorings. *E,E*-**1** and *Z,Z*-**1** in solution exhibited photochromism upon irradiation with visible and UV light, respectively, and this photoisomerization was confirmed by using STM. Furthermore, amorphous films of *Z,Z*-**1** and *E,E*-**1** showed photoisomerization, although single crystals, fibers, and square tubes of *E,E*-**1** remained unchanged under similar conditions. *E,E*-**1** with a 12.5−14.7 Å inner cavity incorporated fullerene C_{60} in the cavity in solution and the solid state to produce a Saturn-like complex, whose structure was determined by X-ray analysis. **2** also formed a Saturn-like complex with C_{60} in the solid state. These Saturn-like complexes are stabilized by van der Waals interactions between the sulfur atoms of 8-mer and C_{60}. The complexes exhibited charge-transfer interactions in the solid state. Like *E,E*-**1**, Saturn-like complex *E,E*-**1**⊃C_{60} formed small cube and fiber structures depending on the solvent used, whereas those of Saturn-like complex **2**⊃C_{60} were limited due to the rigidity of the macroring of **2**.

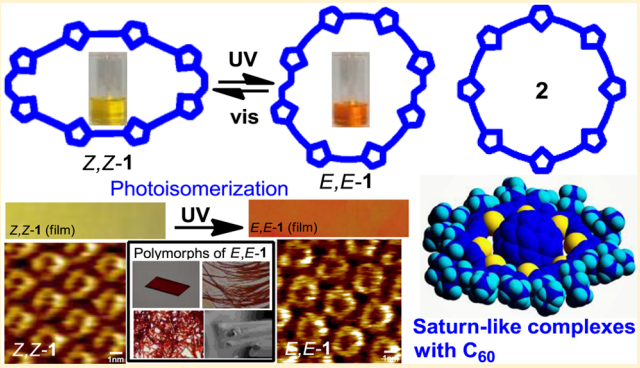

INTRODUCTION

Cyclic benzenoid and nonbenzenoid conjugated molecules have important roles in chemical sciences.[1] Several fully conjugated cyclic molecules have been developed to investigate cyclic conjugation in relation to the Hückel rule,[2] to examine three-dimensional conjugation in belt-shaped molecules,[3] and recently to create molecular machines, sensors, and switches utilizing their electric and optical properties.[4] Among all of the different conjugated cyclic molecules, fully conjugated macrocycles with precisely defined diameters are regarded as being formally infinite π-conjugated systems with inner cavities and outer territories.[5−7] Several macrocycles have inner cavities suitable for including small molecules and metal ions,[8] whereas only a few macrocycles have round-shaped inner cavities of 10−11 Å, which can incorporate large molecules, such as fullerene C_{60} or C_{70}. Following the pioneering study involving the complexation of fullerenes with azacrowns and γ-cyclodextrin,[9] various stable complexes of fullerenes with macrocycles have been reported.[3e,10] In the case of giant macrocycles with cavities > 12 Å, the flexibility of the macrocycles increases and the cavity size becomes too large to incorporate molecules.[1d]

Recently, we constructed macrocyclic oligothiophenes with thiophene, acetylene, and ethylene building blocks.[11,12] We found that the morphology of these macrocyclic oligothiophenes was dependent on the ring size to produce single crystals (cavity size 20 Å), fibrous materials (cavity size 30−40 Å), and microsized powders (cavity size > 50 Å), although their

Received: January 10, 2015
Published: February 20, 2015

DOI: 10.1021/jacs.5b00291
J. Am. Chem. Soc. 2015, 137, 3877−3885

molecular compositions were the same.[11a] Subsequently, we noticed that giant macrocyclic oligothiophenes showed very large two-photon absorption cross sections.[11b] In contrast to giant macrocyclic oligothiophenes, medium-sized rings containing 6−8 thiophene units often exhibit attractive properties due to various mesophases. Quite recently, we found that the 34π-dication of the macrocyclic oligothiophene 6-mer has aromatic cyclic conjugation, whereas the 52π-dication of the macrocyclic oligothiophene 9-mer is nonaromatic and has a bis(radical−cation) structure.[11d] Furthermore, macrocyclic oligothiophene 6-mer shows polymorphism because it has many stable conformations in the solid state due to stabilization from $\pi-\pi$ stacking interactions in the planar structure and destabilization from interatomic repulsions in the inner cavity of the macrocycle. We utilized this polymorphism in switching of FET activity and electrical conductivity and fluorescence switching.

In contrast to the known macrocyclic oligothiophenes, cyclic oligothiophene 8-mer **1**, which has eight thiophene, six acetylene, and two ethylene building blocks, should have an inner cavity of 10−15 Å on the basis of MO calculations. Furthermore, **1** has two geometrical isomers *E,E*-**1** and *Z,Z*-**1** with similar energy levels,[13] and *E,E*-**1**, which is more stable, has a 12.6−14.7 Å inner cavity that can incorporate C_{60} inside to form an inclusion complex. At the same time, we believed that cyclo[8](2,5-thienylene-ethynylene) **2** with eight thiophene and eight acetylene building blocks should exhibit similar structural and inclusion properties. Thus, we synthesized cyclic oligothiophene 8-mers **1** and **2** and found that **1** exhibited photochromic behavior between *E,E*-**1** and *Z,Z*-**1** in solution and the solid state and at the solid−liquid interface. In contrast to the known C_{60} complexes with triangular,[14] square,[15] and belt-shaped macrocycles,[16] *E,E*-**1** and **2** incorporated C_{60} in the cavity to produce Saturn-like complexes. In this paper, we investigated the morphology and photochromic behavior of cyclic oligothiophene 8-mers **1** and **2** and determined the properties of the Saturn-like complexes *E,E*-**1**⊃C_{60} and **2**⊃C_{60}.

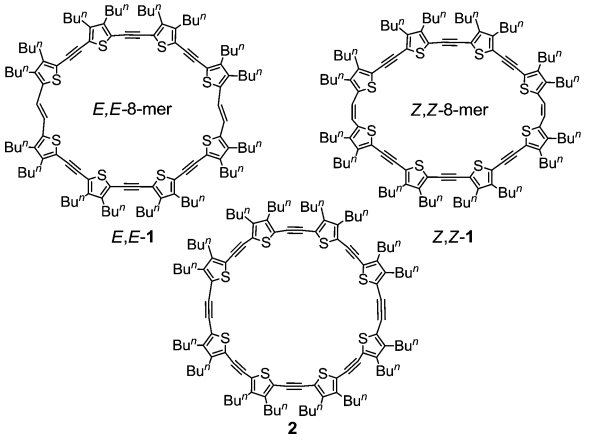

Figure 1. *E,E*-**1**, *Z,Z*-**1**, and **2**.

RESULTS

Synthesis. To synthesize **1**, we employed a McMurry coupling reaction[17] involving **3** composed of four 2,5-thienylene and three ethynylene units under high-dilution conditions in the dark to produce *Z,Z*-**1** (35%) and *E,E*-**1** (1%) with a trace amount of the corresponding 12-mer **4** (Scheme 1).[18] Although *E,E*-**1** is more stable than *Z,Z*-**1**,[13] the reaction

Scheme 1. Synthesis of 1 and 2

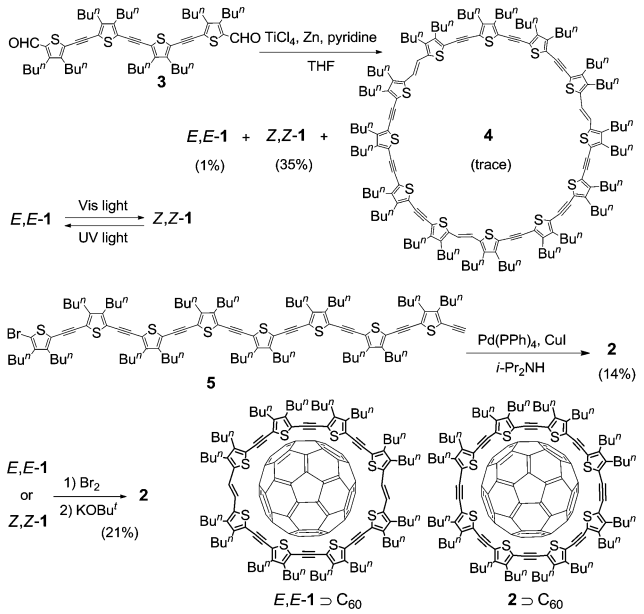

mainly afforded *Z,Z*-**1** as a kinetic product, reflecting the stereochemistry of the bis(*erythro*-diol) intermediate. In contrast, cyclo[8](3,4-dibutyl-2,5-thienylene-ethynylene) **2** was synthesized by intramolecular Sonogashira cyclization of linear ethynyl bromide **5** composed of eight 2,5-thienylene and seven ethynylene core units (14%). Furthermore, bromination of *E,E*-**1** and *Z,Z*-**1**, followed by dehydrobromination with potassium *tert*-butoxide, produced cyclo[8](3,4-dibutyl-2,5-thienylene-ethynylene) **2** in 21% overall yield.[19] *E,E*-**1** and *Z,Z*-**1** are stable red crystalline or amorphous powders and soluble in common organic solvents, except for methanol. *E,E*-**1** easily isomerizes to *Z,Z*-**1** in ambient light, whereas *Z,Z*-**1** slowly isomerizes to *E,E*-**1** under UV irradiation (photochromism).

Structures of *E,E*-1 and 2. Single crystals of *E,E*-**1** were obtained by recrystallization from hot benzene, and its structure was determined by using X-ray analysis. As shown in Figure 2a, *E,E*-**1** has a round structure and lies on a crystallographic center of symmetry. Although DFT calculations on unsubstituted *E,E*-**1** predicted a planar structure,[13] the macroring adopts a nonplanar zigzag conformation (Figure 2b).[20] In the molecular packing, *E,E*-**1** forms a honeycomb, columnar structure and the butyl groups lie above and below the ring, filling the inner cavity of the neighboring rings. The short intermolecular C···C contacts of <3.83 Å between the stacked *E,E*-**1** in the crystal packing are 3.575(7) Å for C(14)···C(15), 3.762(8) Å for C(13)···C(16), and 3.826(6) Å for C(3)···C(12) (Figure 2c).

Single crystals of **2** were obtained by recrystallization from hot benzene. The cell parameters of **2** are similar to those of *E,E*-**1**, indicating that **2** has similar crystal and packing structures to those of **1**. Although the results of DFT calculations on unsubstituted **2** indicate that it has a round, planar structure with D_{8h} symmetry,[21] it adopts a slightly twisted oval structure and the maximum atomic deviation from the least-squares plane of the macroring, excluding the butyl groups, was determined to be 0.0891 Å (Figure 3a and 3b). The

DOI: 10.1021/jacs.5b00291
J. Am. Chem. Soc. 2015, 137, 3877−3885

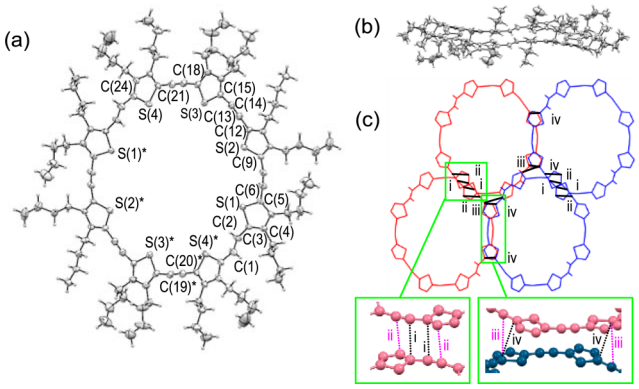

Figure 2. (a) Top view and (b) side view of an ORTEP diagram of *E,E*-**1**. Interatomic distances (Å): S(1)···S(1)* 12.907(2), S(2)···S(2)* 14.486(2), S(3)···S(3)* 14.464(2), S(4)···S(4)* 13.501(2). Thermal ellipsoids are at 50% probability. (c) Packing structure and intermolecular C···C distances (Å) (butyl groups are omitted for clarity): (i) C(14)···C(15) 3.575(7), (ii) C(13)···C(16) 3.762(8), (iii) C(2)···C(12) 4.014(7), (iv) C(3)···C(12) 3.826(6).

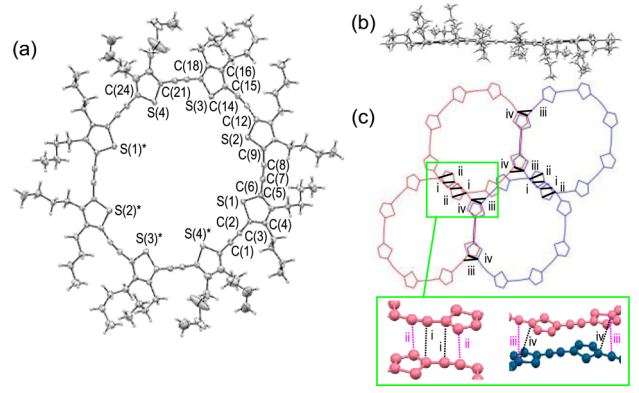

Figure 3. (a) Top view and (b) side view of an ORTEP diagram of **2**. Interatomic distances (Å): S(1)−S(1)* 13.021(3), S(2)−S(2)* 15.377(3), S(3)−S(3)* 14.905(3), S(4)−S(4)* 12.607(2). Thermal ellipsoids are at 50% probability. (c) Packing structure and intermolecular distances (Å) (butyl groups are omitted for clarity): (i) C(14)···C(15) 3.442(6), (ii) C(13)···C(16) 3.431(7), (iii) C(2)···C(12) 3.638(7), (iv) C(3)···C(12) 3.728(6).

C···C contacts shorter than 3.8 Å between the stacked molecules are 3.442(6), 3.431(7), 3.638(7), and 3.728(6) Å for C(14)···C(15), C(13)···C(16), C(2)···C(12), and C(3)···C(12), respectively (Figure 3c). The planarity of **2** facilitates the short C···C contacts among the stacked molecules.

The results of DFT calculations on unsubstituted *E,E*-**1** and **2** indicate that these 8-mers adopt an exactly planar structure, although X-ray single-crystal analysis of *E,E*-**1** and **2** shows slightly bent structures of the macrorings. It is noteworthy that macrocyclic oligothiophenes adopt an essentially planar structure,[11] whereas cycloparaphenylenes (CPPs) adopt a cylindrical form composed of distorted benzene rings.[6] The macrorings of *E,E*-**1** and **2** are more strained than the related 10- and 12-mer;[11] however, the ring strains in *E,E*-**1** and **2** are released by bending ethynylene linkages.[22] The averaged bend angles of Csp−Csp−Csp[2] in *E,E*-**1** and **2** are 172.62° and 174.95°, respectively, and 2,5-thienylene units show almost no strained structures.[23]

Fibrous polymorphs of *E,E*-**1** precipitated from solution, indicating a conformationally restricted macrocyclic structure, which stabilizes various mesophases. As shown in Figure 4, fibers, rods, and square tubes of *E,E*-**1** precipitated from

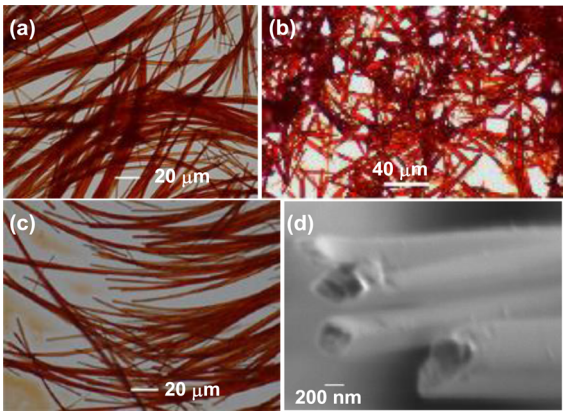

Figure 4. Optical images of (a) fibers from hexane/benzene, (b) rods from $CHCl_3$, and (c) square tubes from benzene/IPE. (d) SEM image of the square tube of *E,E*-**1**.

hexane/benzene (Figure 4a), chloroform (Figure 4b), and benzene/diisopropyl ether (IPE) (Figure 4c and 4d), respectively, without incorporating solvents. The X-ray diffraction (XRD) patterns for the fibers (Figure 5a) corresponded to those for 1-D structures, whereas the XRD patterns for the rods (Figure 5b) and square tubes (Figure 5c and 5d) indicated microcrystalline structures.

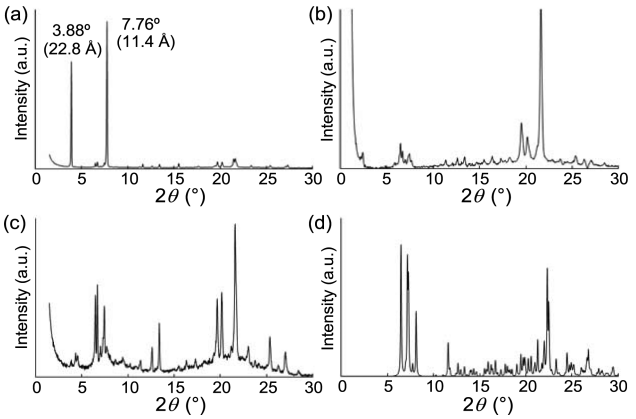

Figure 5. XRD patterns for the (a) fibers, (b) rods, and (c) square tubes on Al plates and (d) a powder sample using the single-crystal data for *E,E*-**1**.

Unlike *E,E*-**1**, **2** only formed cubic single crystals from hot benzene, small rods from benzene, and an amorphous film from THF and CS_2. The XRD patterns for the small rods were similar to those for the single crystals, indicating that they have similar packing structures (Figures S19 and S20, Supporting Information). The rigid planar structure of **2** regulates the morphology.

Photoisomerization between *E,E*-1 and *Z,Z*-1. As described above, in solution, *E,E*-**1** and *Z,Z*-**1** isomerized to *Z,Z*-**1** and *E,E*-**1**, respectively, by irradiation. As shown in Figure 6, *E,E*-**1** and *Z,Z*-**1** exhibit different UV−vis spectra. In other words, irradiation of orange solutions of *E,E*-**1** in cyclohexane, $CHCl_3$, toluene, and benzene with green light (λ = 525 nm) produced *Z,Z*-**1** nearly quantitatively (Scheme 1). On the other hand, irradiation of a yellow solution of *Z,Z*-**1** in cyclohexane

DOI: 10.1021/jacs.5b00291
J. Am. Chem. Soc. 2015, 137, 3877−3885

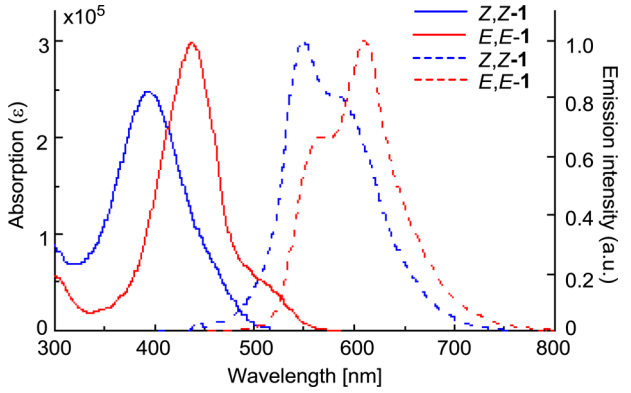

Figure 6. Absorption and emission spectra of *E,E*-**1** and *Z,Z*-**1** in cyclohexane at 25 °C.

with UV light (λ = 365 nm) produced *E,E*-**1** in 96% yield with a trace amount of *E,Z*-**1**.[24] Only *E,E*-**1** crystallized from the solution. In summary, **1** exhibited reversible photochromic behavior between two geometric isomers in solution.

As noted above, *Z,Z*-**1** produced no crystals from common organic solvents but formed an amorphous film on glass and metal surfaces. Moreover, the amorphous film of *Z,Z*-**1** (film A) photoisomerized almost quantitatively to the amorphous film of *E,E*-**1** (film B) by irradiation with UV light at 365 nm (Figure 7a–c), although the amorphous film of *E,E*-**1** could not be

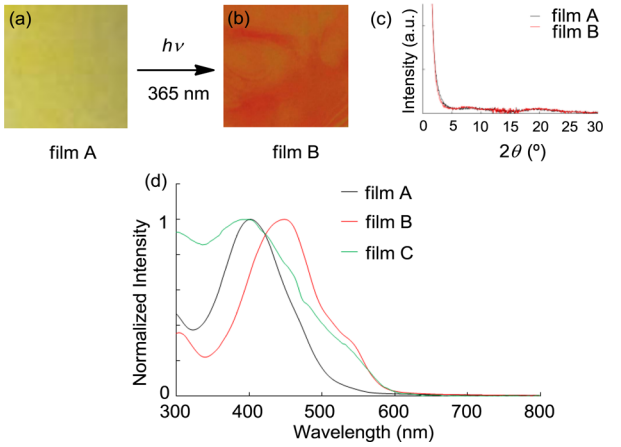

Figure 7. Photoisomerization of amorphous films of (a) *Z,Z*-**1** and (b) *E,E*-**1**. (c) Switching of normalized relative absorption intensities of amorphous films of *Z,Z*-**1** and *E,E*-**1**. (d) Absorption spectra of amorphous films of *Z,Z*-**1** and *E,E*-**1**.

prepared from solutions of *E,E*-**1**. Photoisomerization of film B at 480 nm afforded the amorphous film of *Z,Z*-**1** (film C) in ca. 60% yield (Figure 7d), whereas single crystals, fibers, and square tubes of *E,E*-**1** remained unchanged under similar conditions.

Monolayer Structures of *E,E*-1 and *Z,Z*-1. Scanning tunneling microscope (STM) images at the solid–liquid interface[25,26] were acquired using a custom-made STM with an Omicron controller (Figure 8). Octanoic acid solutions of *E,E*-**1** and *Z,Z*-**1** with concentrations in the range of 10–20 mg/L were applied to the basal plane of freshly cleaved, highly oriented pyrolytic graphite (HOPG), and images were acquired using tips of mechanically cut Pt/Ir wires. Images were corrected with respect to the hexagonal HOPG lattice with SPIP (Image Metrology A/S) image processing software. STM

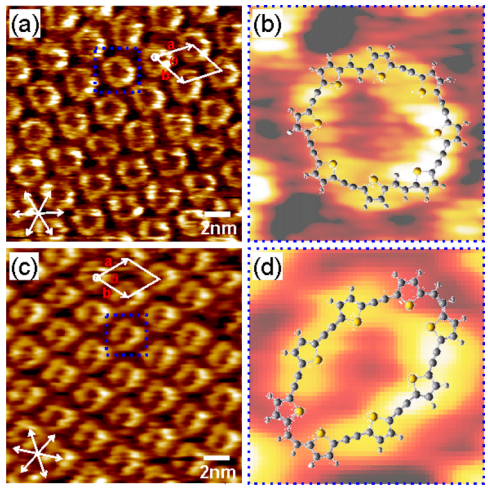

Figure 8. STM height images of a hexagonal network of (a) *E,E*-**1**, unit cell: a = (2.97 ± 0.03) nm, b = (2.95 ± 0.03) nm, θ = (59 ± 3)°, U_t = 1.12 V, I_t = 58 pA, (b) energy minimized structure (B3LYP/6-31G) of *E,E*-**1** superimposed on top of the moiety marked in (a), (c) *Z,Z*-**1**, unit cell: a = (2.83 ± 0.11) nm, b = (2.83 ± 0.09) nm, θ = (60 ± 1)°, U_t = 1.14 V, I_t = 57 pA, (d) energy minimized structure (B3LYP/6-31G) of *Z,Z*-**1** superimposed on top of the moiety marked in (c).

height images of *E,E*-**1** and *Z,Z*-**1** are shown in Figure 8a and 8c. Both *E,E*-**1** and *Z,Z*-**1** self-assembled in a hexagonal close-packed monolayer, and the unit cell parameters for the *E,E*-**1** structure were larger than those for *Z,Z*-**1**. In both images the high-contrast moieties corresponded to the π-electron core of the macrocycles, and due to a large energy difference, the alkyl chains appeared darker and were not fully resolved.[27] The contrasts of the moieties assigned to the macrocycle core were consistent with the optimized DFT structures, as shown in Figure 8b and 8d: *E,E*-**1** appeared as a circular contour, whereas *Z,Z*-**1** appeared as two lobes, closely resembling its ellipsoidal structure. Photoisomerization of *Z,Z*-**1** to *E,E*-**1** and *E,E*-**1** to *Z,Z*-**1** upon irradiation at 365 and 550 nm, respectively, was observed at the solid–liquid interface using the STM. These results will be analyzed in more detail in a further publication.

Electrochemistry. Since cyclic oligothiophenes have relatively high-lying HOMO and HOMO−1 levels, they exhibit multioxidation processes. In the cyclic voltammogram (CV) of *E,E*-**1** (Figure 9a and Table 1), reversible waves corresponding to four one-electron oxidation processes ($E_{1/2}$: 0.22, 0.38, 0.65, and 0.82 V vs Fc/Fc^+) were observed. Similarly, in the CV of **2** (Figure S27, Supporting Information), waves corresponding to three one-electron oxidation processes were observed at slightly more positive potentials in comparison with those of *E,E*-**1** partly because of the replacement of the two vinylene linkages in *E,E*-**1** with the less electron-donating ethynylene linkages. The calculated HOMO levels of *E,E*-**1** and **2** are consistent with those estimated from the first oxidation potentials.[28] In contrast, the CV of *Z,Z*-**1** (Figure 9b) showed characteristic behavior. In the first scan from −0.5 to +0.3 V (red solid line), no anodic current was observed. When the scan range was extended to +0.6 V (blue solid line), a sharp anodic current corresponding to a two-electron process was observed at +0.44 V,[29] which was followed by two cathodic peaks identical to the corresponding peaks of *E,E*-**1**. These results strongly suggested that isomerization of *Z,Z*-**1** to *E,E*-**1** occurred after the formation of a dication.[30] In fact, the first cycle between −0.5 and +1.0 V (black solid line) showed the same anodic current

DOI: 10.1021/jacs.5b00291
J. Am. Chem. Soc. 2015, 137, 3877–3885

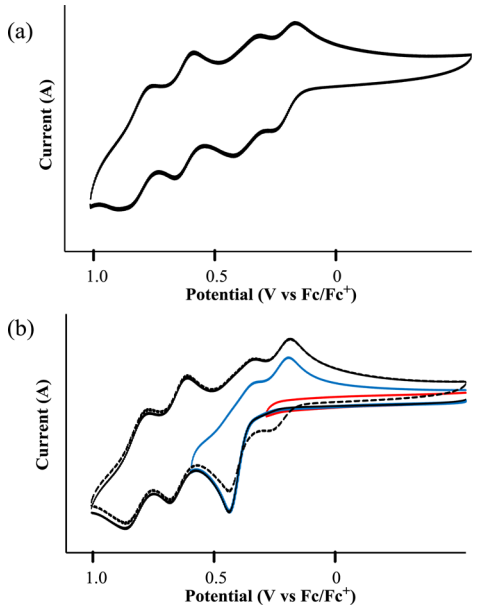

Figure 9. Cyclic voltammograms of (a) *E,E*-**1** (scan range from −0.5 to +1.0 V) and (b) *Z,Z*-**1** (scan ranges (red line) from −0.5 to +0.3 V, (blue line) from −0.5 to +0.6 V, (black solid line) from −0.5 to +1.0 V, (black dashed line) from −0.5 to +1.0 V). Conditions: 0.1 M *n*-Bu_4NPF_6 in 1,2-dichloroethane, Ag/AgCl reference electrode with a Luggin capillary, Pt disk working electrode, Pt wire counter electrode, 0.2 V s^{-1} at 25 °C.

Table 1. Oxidation Potentials[a] of *E,E*-1, *Z,Z*-1, and 2

compd	$E^{ox1}_{1/2}$ (V)	$E^{ox2}_{1/2}$ (V)	$E^{ox3}_{1/2}$ (V)	$E^{ox4}_{1/2}$ (V)	HOMO (eV)[b]	HOMO (eV)[c]
E,E−**1**	0.22, 1e	0.38, 1e	0.65, 1e	0.82, 1e	−5.1	−4.76
Z,Z−**1**	0.44, *d* 2e	*e*	*e*	*e*	*f*	−4.71
2	0.36, 1e	0.51, 1e	0.82, 1e	*e*	−5.2	−4.87

[a]Scan rate: 0.2 V s^{-1} for *E,E*- and *Z,Z*-**1** and 0.1 V s^{-1} for **2**; V vs Fc/Fc^+. [b]HOMO energy value of *E,E*-**1** and **2** was deduced from the measured $E^{ox1}_{1/2}$. [c]HOMO level of unsubstituted *E,E*-**1**, *Z,Z*-**1**, and **2** was estimated at the B3LYP/6-31G(d,p) level. [d]Anodic peak potential. [e]No additional oxidation peak was observed. [f]Not determined.

curve as the blue line until +0.6 V, and then two anodic and four cathodic waves corresponding to those of *E,E*-**1** were observed. Furthermore, in the second cycle (black dashed line), the anodic current corresponding to the first oxidation process of *E,E*-**1** was detected with a scan rate of 0.2 V s^{-1}. Thus, it was concluded that *Z,Z*-**1** isomerized to *E,E*-**1** during the two-electron oxidation process (Figure 9).

Formation and X-ray Structures of Saturn-Like Complexes. Macrocycles with precise shapes and inner cavities form various kinds of C_{60}-containing complexes.[9,14−16] Among them, convex−concave $\pi-\pi$ interactions between the spherical C_{60} and π-conjugated tubular molecules play an important role in stabilizing inclusion complexes, whereas van der Waals interactions between C_{60} and macrocycles help to construct 1:1 inclusion complexes. However, van der Waals interactions are usually too weak to allow for the formation of stable complexes. We found that *E,E*-**1** and **2** incorporate C_{60} in their inner cavities to form unique Saturn-like complexes using van der Waals interactions between C_{60} and the sulfur atoms of oligothiophene 8-mers. In ^{1}H NMR spectra for a 1:1 mixture of *E,E*-**1** and C_{60} in toluene-d_8 (4.00×10^{-3} M) at 25 °C, the peaks for the olefinic protons were shifted downfield by 0.026 ppm in relation to the chemical shift of *E,E*-**1** itself. A Job plot prepared from ^{1}H NMR spectra in toluene-d_8 with a total sample concentration of 2.20×10^{-3} M indicated that a 1:1 complex formed, and the binding constant (K_a) for *E,E*-**1** with C_{60} in toluene-d_8 at −20 °C was determined to be 439 ± 14.8 M^{-1}, whereas K_a at 40 °C was 56 ± 12.6 M^{-1} (ΔH = −22.8 kJ mol^{-1} K^{-1}; ΔS = −38.8 J mol^{-1} K^{-1}). These results showed that only 3.5% of *E,E*-**1** formed a complex with C_{60} in toluene (4.00×10^{-4} M) at 25 °C, whereas more than 83% of *E,E*-**1** formed a complex in the same toluene solution at −100 °C. In the UV−vis−NIR spectrum for the 1:1 mixture of *E,E*-**1** and C_{60} in toluene, a broad charge-transfer absorption was observed in the range of 600−800 nm. In the case of **2**, however, K_a could not be accurately determined from the analysis of the ^{1}H NMR and UV−vis spectra due to small differences between the spectra for **2** and its C_{60} complex.

In contrast to the weak interactions between *E,E*-**1** and **2** and C_{60} in solution, these macrocycles formed stable C_{60} complexes in the solid state. When a solution of *E,E*-**1** and C_{60} (1:1) in hot toluene was allowed to stand at room temperature overnight, black cubic single crystals formed and the structure was determined by using X-ray analysis. The most striking characteristic of *E,E*-**1**⊃C_{60} is its Saturn-like structure, in which the C_{60} core is surrounded by the planar *E,E*-**1** ring (Figure 10a and 10b). The face-to-face S···S distances (13.607(2)−14.661(3) Å, average S···S distance 13.99 Å) indicate that the oligothiophene ring is nearly circular, and the short S···S distances (13.607 and 13.661 Å) are 1.0% shorter than the sum (13.72 Å) of the van der Waals radii of the sulfur atoms (3.70 Å) and C_{60} (10.02 Å).[31] The short contacts

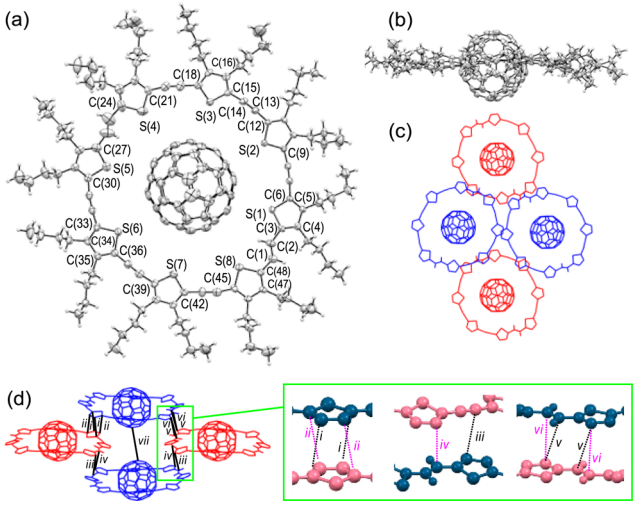

Figure 10. (a) Top view, (b) side view, and packing structures along (c) the *a* axis and (d) the *c* axis of an ORTEP diagram of *E,E*-**1**⊃C_{60} (butyl groups are omitted for clarity). Thermal ellipsoids are at 50% probability. Interatomic distances (Å): S(1)···S(5) = 13.660(3), S(2)···S(6) = 13.607(2), S(3)···S(7) = 14.045(2), S(4)···S(8) = 14.661(3), S(1)···C(C_{60}) = 3.575(5), S(2)···C(C_{60}) = 3.772(8), S(3)···C(C_{60}) = 3.527(6), S(4)···C(C_{60}) = 3.758(8), S(5)···C(C_{60}) = 3.858(6), S(6)···C(C_{60}) = 3.737(6), S(7)···C(C_{60}) = 3.742(6), S(8)···C(C_{60}) = 4.144(8). Intermolecular distances (Å): (*i*) C(14)···C(15) 3.442(6), (*ii*) C(13)···C(16) 3.431(7), (*iii*) C(33)···C(35) 3.580(7), (*iv*) C(34)···C(36) 3.617(7), (*v*) C(1)···C(47) 3.687(7), (*vi*) C(2)···C(47) 3.774(7), (*vii*) C(C_{60})···C(C_{60}) 5.883(8).

DOI: 10.1021/jacs.5b00291
J. Am. Chem. Soc. 2015, 137, 3877−3885

between the sulfur atoms and C_{60} stop the rotation of C_{60}, which is different from complexes with convex−concave $\pi-\pi$ interactions (a ball-bearing system).[3a,f,32] In the crystal packing, there are six short C···C contacts of <3.77 Å between the stacked *E,E*-**1** (*i* 3.431(7) Å and *ii* 3.774(7) Å) (Figure 10c and 10d). However, the closest C_{60}···C_{60} distance in the single crystal (*vii* 5.883(8) Å) suggests that there are almost no $\pi\cdots\pi$ interactions between C_{60} molecules.

Single crystals of **2**⊃C_{60} were obtained by crystallization of a mixture of **2** and C_{60} (1:1) in hot toluene, and its structure was determined by using X-ray analysis (Figure 11). In one of the

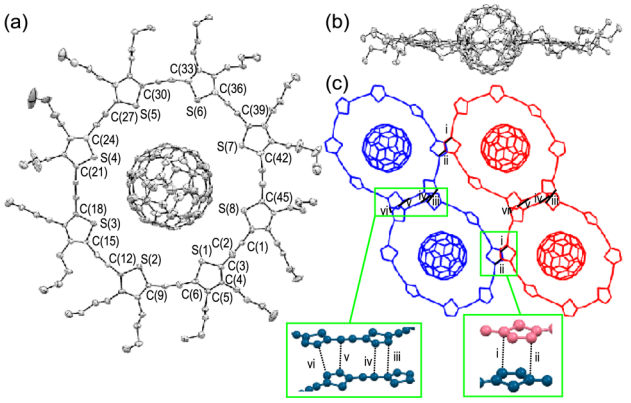

Figure 11. (a) Top view and (b) side view of an ORTEP diagram of **2**⊃C_{60} (H atoms are omitted for clarity.). Thermal ellipsoids are at 50% probability. (c) Packing structure along the *c* axis of **2**⊃C_{60} (butyl groups are omitted for clarity). Interatomic distances (Å): S(1)···S(5) = 14.137(6), S(2)···S(6) = 14.668(6), S(3)···S(7) = 13.908(5), S(4)···S(8) = 13.617(4), S(1)···C(C_{60}) = 3.78(2), S(2)···C(C_{60}) = 3.91(2), S(3)···C(C_{60}) = 3.59(1), S(4)···C(C_{60}) = 3.58(1), S(5)···C(C_{60}) = 4.11(2), S(6)···C(C_{60}) = 4.49(2), S(7)···C(C_{60}) = 3.63(1), S(8)···C(C_{60}) = 3.49(2). Intermolecular C···C distances (Å): (*i*) C(4)···C(30) 3.41(1), (*ii*) C(6)···C(28) 3.42(1), (*iii*) C(10)···C(39) 3.68(1), (*iv*) C(11)···C(38) 3.65(1), (*v*) C(14)···C(35) 3.67(1), (*vi*) C(16)···C(34) 3.67(1), (*vii*) C(C_{60})···C(C_{60}) 5.81(2).

two independent **2**⊃C_{60} complexes in the crystal, the positions of some of the carbon atoms of C_{60} could not be determined due to disorder. In the other complex, the face-to-face S···S distances (13.617(5)−14.668(6) Å, average S···S distance 14.08 Å) indicate that it has a round shape, and the short S···S distance (13.617 Å) is 1.0% shorter than the sum of the van der Waals radii of the sulfur atoms (13.72 Å) and C_{60}. Therefore, the intermolecular interactions between **2** and C_{60} are slightly weaker than those in *E,E*-**1**⊃C_{60}. The shortest C···C contact between the stacked **2**⊃C_{60} (*i* 3.41(1) Å) and the closest C_{60}···C_{60} distance in the column (*vii* 5.81(2) Å) are similar to those of *E,E*-**1**⊃C_{60} (Figure 11c). Thus, the small structural differences between *E,E*-**1** and **2** barely affect the intra- and intermolecular distances in the C_{60} complexes.

Polymorphism of the Saturn-Like Complexes. The Saturn-like complex *E,E*-**1**⊃C_{60} formed fibrous and cubic polymorphs, which precipitate from solution (Figure 12a and 12b). Casting of a CS_2 solution of *E,E*-**1**⊃C_{60} produced fibers, whereas similar casting of a benzene solution formed small cubes. In Figure 12c, the strong (001) reflection of the fiber at 2θ = 4.85° (*d* = 18.2 Å) was ascribed to the molecular size, whereas the weak reflections at 2θ = 9.69° (002) and 14.54° (003) were ascribed to higher order complexes. Since the molecular diameter of *E,E*-**1** was estimated to be 31.6 Å, the

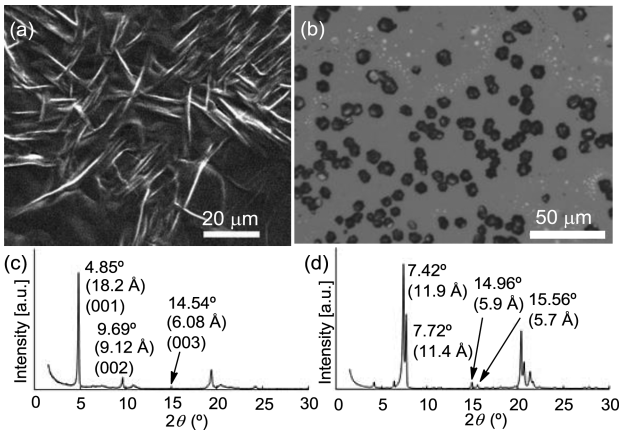

Figure 12. (a) SEM image of fibers of *E,E*-**1**⊃C_{60} obtained from CS_2. (b) Optical image of small cubes of *E,E*-**1**⊃C_{60} obtained from benzene. XRD patterns for (c) the fibers and (d) the small cubes of *E,E*-**1**⊃C_{60} on an Al plate.

XRD pattern indicates that the film has a laterally ordered lamellar structure (*d* = 18.2 Å) rising 35° diagonally from the aluminum plate used for the XRD analysis of the fiber. On the other hand, the small cubes showed simple but similar patterns to those of powdered single crystals of *E,E*-**1**⊃C_{60} (Figure 12d and Figures S38 and S39, Supporting Information). The UV−vis spectra for the single crystals, fibers, and small cubes of *E,E*-**1**⊃C_{60} were similar, meaning that they each had weak CT interactions between *E,E*-**1** and C_{60} in the solid state (Figure S40, Supporting Information). Similarly to single crystals, fibers, rods, and square tubes of *E,E*-**1**, single crystals, fibers, and small cubes of *E,E*-**1**⊃C_{60} show no photoisomerization and remain unchanged upon irradiation at 480 nm.

Saturn-like complex **2**⊃C_{60} formed single crystals in hot toluene and small cubes in benzene. The XRD patterns for both polymorphs were similar. From UV−vis−NIR spectra for **2**⊃C_{60}, there are weak CT absorptions (λ_{abs} 600−800 nm) between **2** and C_{60}, confirming that a similar complex forms in the solid state. In contrast, when CS_2 was used, **2** and C_{60} (1:1) formed an amorphous film and the UV−vis−NIR spectrum of the amorphous film exhibited no CT absorption band, meaning that **2** did not form a Saturn-like complex with C_{60} on the surface (Figures S42 and S43, Supporting Information)[30] due to weak intermolecular interactions. In other words, the rigid planar structure of **2** affects the formation of different polymorphs.

■ CONCLUSION

Medium-sized macrocyclic oligothiophene 8-mers *E,E*-**1** and *Z,Z*-**1** with similar energy levels were synthesized by selective cyclodimerization of thiophene dialdehyde **3** containg four 2,5-thienylene and three ethynylene core units with a low-valent titanium reagent. On the other hand, cyclo[8](2,5-thienylene-ethynylene) **2** was synthesized either by intramolecular Sonogashira cyclization of ethynyl bromide **5** containing eight 2,5-thienylene and seven ethynylene core units or by a bromination−dehydrobromination procedure of *E,E*-**1** and *Z,Z*-**1**. From X-ray analysis, *E,E*-**1** had a round, zigzag conformation whereas **2** had a round, planar structure. The structural flexibility and the mesophase in *E,E*-**1** make nanostructured polymorphs, such as fibers, rods, and square tubes, possible. On the other hand, the rigid, planar structure of **2** limits morphological variety, and only small rectangular plates

DOI: 10.1021/jacs.5b00291
J. Am. Chem. Soc. 2015, 137, 3877−3885

and amorphous films formed. Self-assembled monolayers of *E,E*-**1** and *Z,Z*-**1** were constructed as hexagonal porous networks under STM conditions at the solid−liquid interface. Photoisomerization between *E,E*-**1** and *Z,Z*-**1** was observed in solution, in the solid state, and at the solid−liquid interface. In solution, *E,E*-**1** and *Z,Z*-**1** exhibited photochromism upon irradiation with visible (525 nm) and UV light (365 nm), respectively. Moreover, at the solid−liquid interface, the self-assembled networks of *E,E*-**1** and *Z,Z*-**1** photoisomerized upon irradiation with visible (550 nm) and UV light (365 nm), respectively. Furthermore, an amorphous film of *Z,Z*-**1** photoisomerized by irradiation with UV light at 365 nm, and the resulting amorphous film of *E,E*-**1** isomerized back into the amorphous *Z,Z*-**1** film when it was irradiated with visible light at 480 nm. In contrast, single crystals, fibers, rods, and square tubes of *E,E*-**1** were stable and did not photoisomerize when irradiated with visible light at 480 nm. In the CV measurements, *E,E*-**1**, *Z,Z*-**1**, and **2** showed multioxidation process. A two-electron oxidation of *Z,Z*-**1** first produced $(Z,Z\text{-}\mathbf{1})^{2+}$, which easily isomerized to the more stable $(E,E\text{-}\mathbf{1})^{2+}$ under the CV conditions.

Oligothiophene 8-mers *E,E*-**1** and **2** incorporated C_{60} to form new Saturn-like complexes. From X-ray analysis, the inner cavities of both *E,E*-**1** and **2** have optimal sizes for incorporating C_{60}. Although *E,E*-**1** and **2** weakly incorporated C_{60} in solution, from X-ray analysis, some of the S···S distances in Saturn-like *E,E*-**1**⊃C_{60} and **2**⊃C_{60} were determined to be a little shorter than the sum of the van der Waals radii of the sulfur atoms and C_{60}. As a result, the sulfur atoms of the thiophene rings interact with C_{60} to hinder its rotation. Furthermore, *E,E*-**1**⊃C_{60} formed various nanostructured polymorphs, such as single crystals, fibers, and small cubes. However, the number of polymorphs of **2**⊃C_{60} was limited due to the rigid, planar structure of **2**. These new donor−acceptor Saturn-like complexes have potential applications as molecular machines and switches by utilizing their electric and optical properties.

■ ASSOCIATED CONTENT

Supporting Information

Experimental procedures and characterization data of *E,E*-**1**, *Z,Z*-**1**, **2**−**5**, *E,E*-**1**⊃C_{60} and **2**⊃C_{60}; ^{1}H and ^{13}C NMR spectra (Figures S1−S5), HOMO and LUMO orbitals and optimized structures (Figures S6−S11), X-ray analysis of *E,E*-**1** and **2** (Figures S12−S13 and Table S1), absorption and emission spectra of *E,E*-**1**, *Z,Z*-**1**, **2**, and **4** (Figure S14 and Table S2), polymorphism of *E,E*-**1**, *Z,Z*-**1**, and **2** (Figures S15−S21 and Tables S3−S4), photoisomerization (Figures S22−S25), STM (Figure S26), redox behavior (Figures S27−S28 and Table S5), *E,E*-**1**⊃C_{60} formation (Figures S29−S35 and Table S6), X-ray analysis of *E,E*-**1**⊃C_{60} and **2**⊃C_{60} (Figures S36−S37 and Table S7), morphlogy of *E,E*-**1**⊃C_{60} and **2**⊃C_{60} (Figures S38−S44), calculated strain erergies (Figure S45 and Table S8), synthetic procedures (Schemes S1−S3), Cartesian coordinates and total energies of the optimized structures of *E,E*-**1**, *Z,Z*-**1**, **2**, *E,E*-**1**⊃C_{60}, **2**⊃C_{60}, $E,E\text{-}\mathbf{1}^{2+}$ and $Z,Z\text{-}\mathbf{1}^{2+}$ (B3LYP/6-31G(d,p)) (Tables S9−S15), and crystallographic information files (CIF) for *E,E*-**1**, **2**, *E,E*-**1**⊃C_{60}, and **2**⊃C_{60}. This material is available free of charge via the Internet at http://pubs.acs.org.

■ AUTHOR INFORMATION

Corresponding Author

*iyoda@tmu.ac.jp

Notes

The authors declare no competing financial interest.

■ ACKNOWLEDGMENTS

This work was supported by JST, Strategic International Research Cooperative Program (SICP) [Strategic Japanese-German Cooperation Program from JST], the German Science Foundation (DFG) Ra482/6-1, and Grant-in-Aid for Scientific Research from JSPS. We would Ms. Chika Tabata, Mr. Tomoya Tamachi, and Dr. Jun Yamakawa (Tokyo Metropolitan University) for their experimental assistance. We also thank Prof. Hirohisa Yoshida and Mr. Jang Junhyeok (Tokyo Metropolitan University) for their assistance with DSC and XRD measurements. We are thankful to Prof. Biao Zhou (Nihon University), Prof. Akiko Kobayashi (Nihon University), Prof. Kotohiro Nomura (Tokyo Metropolitan University), and Prof. Yoshio Aso (Osaka University) for helpful discussions.

■ REFERENCES

(1) For recent reviews: (a) Spitler, E. L.; Johnson, C. A., II; Haley, M. M. *Chem. Rev.* **2006**, *106*, 5344−5386. (b) Gholami, M.; Tyhwinski, R. R. *Chem. Rev.* **2006**, *106*, 4997−5027. (c) Mishra, A.; Ma, C.-Q.; Bäuerle, P. *Chem. Rev.* **2009**, *109*, 1141−1276. (d) Iyoda, M.; Yamakawa, J.; Rahman, M. J. *Angew. Chem., Int. Ed.* **2011**, *50*, 10522−10553.

(2) For reviews, see: (a) Mitchell, R. H. *Chem. Rev.* **2001**, *101*, 1301−1315. (b) Kennedy, R. D.; Lloyd, D.; McNab, H. *J. Chem. Soc., Perkin Trans 1* **2002**, 1601−1621. (c) Marsella, M. J. *Acc. Chem. Res.* **2002**, *35*, 944−951. (d) Marsden, J. A.; Palmer, G. J.; Haley, M. M. *Eur. J. Org. Chem.* **2003**, 2355−2369. (e) Nishinaga, T. *Sci. Synth.* **2009**, *45a*, 407−427.

(3) For reviews, see: (a) Kawase, T.; Kurata, H. *Chem. Rev.* **2006**, *106*, 5250−5273. (b) Kawase, T.; Oda, M. *Pure Appl. Chem.* **2006**, *77*, 831−839. (c) Tahara, K.; Tobe, Y. *Chem. Rev.* **2006**, *106*, 5274−5290. (d) Eisenberg, D.; Shenhar, R.; Rabinovitz, M. *Chem. Soc. Rev.* **2010**, *39*, 2879−2890. (e) Hirst, E. S.; Jasti, R. *J. Org. Chem.* **2012**, *77*, 10473−10478. (f) Matsuno, T.; Naito, H.; Hitosugi, S.; Sato, S.; Kotani, M.; Isobe, H. *Pure Appl. Chem.* **2014**, *86*, 489−495.

(4) For reviews, see: (a) Guo, X.; Baumgarten, M.; Müllen, K. *Prog. Polym. Sci.* **2013**, *38*, 1832−1908. (b) Hsu, L.-Y.; Rabitz, H. *Phys. Rev. Lett.* **2012**, *109*, 186801(5). (c) Martínez-Díaz, M. V.; De La Torre, G.; Torres, T. *Chem. Commun.* **2010**, *46*, 7090−7108. (c) Cuesta, L.; Sessler, J. L. *Chem. Soc. Rev.* **2009**, *38*, 2716−2729. (d) Babudri, F.; Farinola, G. M.; Naso, F. *J. Mater. Chem.* **2004**, *14*, 11−34.

(5) For macrocyclic oligothiophenes, see: (a) Zhang, F.; Götz, G.; Mena-Osteritz, E.; Weil, M.; Sarkar, B.; Kaim, W.; Bäuerle, P. *Chem. Sci.* **2011**, *2*, 781−784. (b) Zhang, F.; Götz, G.; Winkler, H. D. F.; Schalley, C. A.; Bäuerle, P. *Angew. Chem., Int. Ed.* **2009**, *48*, 6632−6635. (c) Fuhmann, G.; Debaerdemaeker, T.; Bäuerle, P. *Chem. Commun.* **2003**, 948−949. (d) Mena-Osteritz, E.; Bäuerle, P. *Adv. Mater.* **2001**, *13*, 243−246. (e) Krömer; Rios-Carreras, I.; Fuhrmann, G.; Musch, C.; Wunderlin, M.; Debaerdemaeker, T.; Mena-Osteritz, E.; Bäuerle, P. *Angew. Chem., Int. Ed.* **2000**, *39*, 3481−3486.

(6) For recent examples of macrocyclic oligophenylenes, see: (a) Kayahara, E.; Patel, V. K.; Yamago, S. *J. Am. Chem. Soc.* **2014**, *136*, 2284−2287. (b) Iwamoto, T.; Kayahara, E.; Yasuda, N.; Suzuki, T.; Yamago, S. *Angew. Chem., Int. Ed.* **2014**, *53*, 6430−6434. (c) Golling, F. E.; Quernheim, M.; Wagner, M.; Nishiuchi, T.; Müllen, K. *Angew. Chem., Int. Ed.* **2014**, *53*, 1525−1528. (d) Wang, K.; Wang, C.-Y.; Zhang, Y.; Zhang, S. X.-A.; Yang, B.; Yang, Y.-W. *Chem. Commun.* **2014**, *50*, 9458−9461. (e) Yagi, A.; Venkataramana, G.; Segawa, Y.; Itami, K. *Chem. Commun.* **2014**, *50*, 957−959. (f) Ishii, Y.; Matsuura, S.; Segawa, Y.; Itami, K. *Org. Lett.* **2014**, *16*, 2174−2176. (g) Huang, C.; Huang, Y.; Akhmedov, N. G.; Popp, B. V.; Petersen, J. L.; Wang, K. K. *Org. Lett.* **2014**, *16*, 2672−267. (h) Adamska, L.; Nayyar, I.; Chen, H.; Swan, A. K.; Oldani, N.; Fernandez-Alberti, S.; Golder, M. R.; Jasti, R.; Doorn, S. K.; Tretiak, S. *Nano Lett.* **2014**, *14*,

DOI: 10.1021/jacs.5b00291
J. Am. Chem. Soc. 2015, 137, 3877−3885

6539−6546. (i) Hines, D. A.; Darzi, E. R.; Jasti, R.; Kamat, P. V. *J. Phys. Chem. A* **2014**, *118*, 1595−1600. (j) Evans, P. J.; Darzi, E. R.; Jasti, R. *Nat. Chem.* **2014**, *6*, 404−408. (k) Kameoka, Y.; Sato, T.; Koyama, T.; Tanaka, K.; Kato, T. *Chem. Phys. Lett.* **2014**, *598*, 69−74.

(7) For π-extended macrocycles, see: (a) Standera, M.; Häflinger, R.; Gershoni-Poranne, R.; Stanger, A.; Jeschke, G.; van Beek, J. D.; Bertschi, L.; Schlüter, A. D. *Chem.—Eur. J.* **2011**, *17*, 12163−12174. (b) Hanai, Y.; Rahman, M. J.; Yamakawa, J.; Takase, M.; Nishinaga, T.; Hasegawa, M.; Kamada, K.; Iyoda, M. *Chem.—Asian J.* **2011**, *11*, 2940−2945. (c) Schwab, M. G.; Qin, T.; Pisula, W.; Mavrinskiy, A.; Feng, X.; Baumgarten, M.; Kim, H.; Laquai, F.; Schuh, S.; Trattnig, R.; List, E. J. W.; Müllen, K. *Chem.—Asian J.* **2011**, *11*, 3001−3010. (d) Shibata, T.; Fujimoto, M.; Hirashima, H.; Chiba, T.; Endo, K. *Synthesis* **2012**, *44*, 3269−3284. (e) Nishiuchi, T.; Feng, X.; Enkelmann, V.; Wagner, M.; Müllen, K. *Chem.—Eur. J.* **2012**, *18*, 16621−16625.

(8) For recent reviews, see: (a) Iyoda, M.; Kuwatani, Y.; Nishinaga, T.; Takase, M.; Nishiuchi, T. In *Fragments of Fullerenes and Carbon Nanotubes*; Petrukhina, M. A., Scott, L. T., Eds.; John Wiley & Sons: New York, 2011. (b) Guo, D.-S.; Liu, Y. *Chem. Soc. Rev.* **2012**, *41*, 5907−5921. (c) Frischmann, P. D.; MacLachlan, M. J. *Chem. Soc. Rev.* **2013**, *42*, 871−890. (d) Fabbrizzi, L.; Poggi, A. *Chem. Soc. Rev.* **2013**, *42*, 1681−1699.

(9) (a) Diederich, F.; Effing, J.; Jonas, U.; Jullien, L.; Plesnivy, T.; Ringsdorf, H.; Thilgen, C.; Weinstein, D. *Angew. Chem., Int. Ed.* **1992**, *31*, 1599−1602. (b) Andersson, T.; Nilsson, K.; Sundahl, M.; Westman, G.; Wennerström, O. *Chem. Commun.* **1992**, 604−606. (c) Yoshida, Z.-i.; Takekuma, H.; Takekuma, S.-i.; Matsubara, Y. *Angew. Chem., Int. Ed.* **1994**, *33*, 1597−1599.

(10) For recent reviews: (a) Tashiro, K.; Aida, T. *Chem. Soc. Rev.* **2007**, *36*, 189−197. (b) Pérez, E. M.; Martín, N. *Chem. Soc. Rev.* **2008**, *37*, 1512−1519. (c) Canevet, D.; Pérez, E. M.; Martín, N. *Angew. Chem., Int. Ed.* **2011**, *50*, 9248−9259.

(11) (a) Nakao, K.; Nishimura, M.; Tamachi, T.; Kuwatani, Y.; Miyasaka, H.; Nishinaga, T.; Iyoda, M. *J. Am. Chem. Soc.* **2006**, *128*, 16740−16747. (b) Williams-Harry, M.; Bhaskar, A.; Ramakrishna, G.; Goodson, T., III; Imamura, M.; Mawatari, A.; Nakao, K.; Enozawa, H.; Nishinaga, T.; Iyoda, M. *J. Am. Chem. Soc.* **2008**, *130*, 3252−3253. (c) Donehue, J. E.; Varnavski, O. P.; Cemborski, R.; Iyoda, M.; Goodson, T., III *J. Am. Chem. Soc.* **2011**, *133*, 4819−4828. (d) Iyoda, M.; Tanaka, K.; Shimizu, H.; Hasegawa, M.; Nishinaga, T.; Nishiuchi, T.; Kunugi, Y.; Ishida, T.; Otani, H.; Sato, H.; Inukai, K.; Tahara, K.; Tobe, Y. *J. Am. Chem. Soc.* **2014**, *136*, 2389−2396.

(12) (a) Iyoda, M. *Pure Appl. Chem.* **2010**, *82*, 831−841. (b) Iyoda, M. *C. R. Chim.* **2009**, *12*, 395−402. (c) Iyoda, M. *Heteroat. Chem.* **2007**, *18*, 460−466. (d) Iyoda, M. *J. Synth. Org. Chem. Jpn.* **2012**, *70*, 1157−1163.

(13) Unsubstituted *E,E*-**1** is 5.0 kcal mol^{-1} more stable than unsubstituted *Z,Z*-**1** based on the calculation at the B3LYP/6-31G(d,p) level (Figure S6, Supporting Information).

(14) (a) Gil-Ramírez, G.; Karlen, S. D.; Shundo, A.; Porfyrakis, K.; Ito, Y.; Briggs, G. A. D.; Morton, J. J. L.; Anderson, H. L. *Org. Lett.* **2010**, *12*, 3544−3547. (b) Mulholland, A. R.; Woodward, C. P.; Langford, S. J. *Chem. Commun.* **2011**, *47*, 1494−1496. (c) Rahman, M. J.; Shimizu, H.; Araki, Y.; Ikeda, H.; Iyoda, M. *Chem. Commun.* **2013**, *49*, 9251−9253.

(15) (a) Tashiro, K.; Aida, T.; Zheng, J.-Y.; Kinbara, K.; Saigo, K.; Sakamoto, S.; Yamaguchi, K. *J. Am. Chem. Soc.* **1999**, *121*, 9477−9478. (b) Wang, M.-X.; Zhang, X.-H.; Zheng, Q.-Y. *Angew. Chem., Int. Ed.* **2004**, *43*, 838−842. (c) Kieran, A. L.; Pascu, S. I.; Jarrosson, T.; Sanders, J. K. M. *Chem. Commun.* **2005**, *41*, 1276−1278. (d) Nobukuni, H.; Shimazaki, Y.; Tani, F.; Naruta, Y. *Angew. Chem., Int. Ed.* **2007**, *46*, 8975−8978. (e) Yamaguchi, Y.; Kobayashi, S.; Amita, N.; Wakamiya, T.; Matsubara, Y.; Sugimoto, K.; Yoshida, Z.-i. *Tetrahedron Lett.* **2002**, *43*, 3277−3280. (f) Song, J.; Aratani, N.; Shinokubo, H.; Osuka, A. *J. Am. Chem. Soc.* **2010**, *132*, 16356−16357.

(16) (a) Kawase, T.; Tanaka, K.; Fujiwara, N.; Darabi, H. R.; Oda, M. *Angew. Chem., Int. Ed.* **2003**, *42*, 1624−1628. (b) Kawase, T.; Tanaka, K.; Shiono, N.; Seirai, Y.; Oda, M. *Angew. Chem., Int. Ed.* **2004**, *43*, 1722−1724. (c) Isla, H.; Gallego, M.; Pérez, E. M.; Viruela, R.; Ortí, E.; Martín, N. *J. Am. Chem. Soc.* **2010**, *132*, 1772−1773. (d) Iwamoto, T.; Watanabe, Y.; Sadahiro, T.; Haino, T.; Yamago, S. *Angew. Chem., Int. Ed.* **2011**, *50*, 8342−8344. (e) Xia, J.; Bacon, J. W.; Jasti, R. *Chem. Sci.* **2012**, *3*, 3018−3021. (f) Isobe, H.; Hitosugi, S.; Yamasaki, T.; Iizuka, R. *Chem. Sci.* **2013**, *4*, 1293−1297. (g) Hitosugi, S.; Iizuka, R.; Yamasaki, T.; Zhang, R.; Murata, Y.; Isobe, H. *Org. Lett.* **2013**, *15*, 3199−3201. (h) Miki, K.; Matsushita, T.; Inoue, Y.; Senda, Y.; Kowada, T.; Ohe, K. *Chem. Commun.* **2013**, *49*, 9092−9094. (i) Hitosugi, S.; Ohkubo, K.; Iizuka, R.; Kawashima, Y.; Nakamura, K.; Sato, S.; Kono, H.; Fukuzumi, S.; Isobe, H. *Org. Lett.* **2014**, *16*, 3352−3355. (j) Sato, S.; Yamasaki, T.; Isobe, H. *Proc. Natl. Acad. Sci. U.S.A.* **2014**, *111*, 8374−8379.

(17) For a recent review: Heravi, M. M.; Faghihi, Z. *Curr. Org. Chem.* **2012**, *16*, 2097−2123.

(18) For the McMurry coupling reaction, a solution of **3** in THF−pyridine was added to a solution of low-valent titanium reagent (11 equiv) in refluxing THF for 24 h (Supporting Information).

(19) Linear ethynylbromide **5** was prepared from 3,4-dibutyl-2-iodo-5-trimethylsilylethynylthiophene in six steps in 58% overall yield (Supporting Information).

(20) Flexible macrorings easily form various crystal structures depending on weak interactions in the crystal lattice. For example, a butyl-substituted macrocyclic oligothiophene 4-mer has an extremely twisted structure to accommodate eight butyl groups in the crystal lattice.[34] However, the corresponding unsubstituted molecule is planar,[35] because π−π stacking interaction in the crystal lattice overcomes destabilization of the planar structure.[36]

(21) Unsubstituted **2** has a round, planar structure on the calculation at the B3LYP/6-31G(d,p) level (Figure S10, Supporting Information).

(22) The bend angles of Csp−Csp−Csp^2 linkages determined by X-ray analysis are as follows. *E,E*-**1**, 170.63−176.17°; **2**, 168.74−177.77°.

(23) DFT calculations on the strain energies of the unsubstituted 8-mers showed that *E,E*-**1** and **2** have 10.01 and 6.09 kcal mol^{-1} strain energies based on ring formation, but *Z,Z*-**1** exhibits almost no additional strain energy by ring formation. Since the cis-double bonds in *Z,Z*-**1** are destabilized by 14.37 kcal mol^{-1} as compared with trans-double bonds, unsubstituted *E,E*-**1** is by 5.0 kcal mol^{-1} more stable than unsubstituted *Z,Z*-**1** (Figure S45 and Table S8, Supporting Information).

(24) Photoisomerization between *E,E*-**1** and *Z,Z*-**1** is two-step reaction, and a trace amount of *E,Z*-**1** was observed as a byproduct of the reaction. However, *E,Z*-**1** was unstable, and attempted isolation was unsuccessful (Figure S6, Supporting Information). The unsubstituted *E,Z*-**1** is by 7.2 kcal mol^{-1} less stable than unsubstituted *E,E*-**1** based on the calculation at the B3LYP/6-31G(d,p) level.

(25) (a) Rabe, J. P.; Buchholz, S. *Science* **1991**, *253*, 424−427. (b) Rabe, J. P.; Buchholz, S. *Phys. Rev. Lett.* **1991**, *66*, 2096−2099.

(26) Seifert, C.; Skuridina, D.; Dou, X.; Müllen, K.; Severin, N.; Rabe, J. P. *Phys. Rev. B* **2009**, *80*, 245429.

(27) Lazzaroni, R.; Calderone, A.; Brédas, J. L.; Rabe, J. P. *J. Chem. Phys.* **1997**, *107*, 99−105.

(28) The estimated HOMO levels from the first oxidation potentials of *E,E*-**1** and **2** were calculated based on the energy level of the F_c/F_c^+ couple to vacuum (−4.84 eV).[37]

(29) One-step, two-electron process at a peak potential of +0.44 V in the CV of **2** was assigned based on the peak height, high oxidation potential despite the high calculated HOMO, and the similarity to the corresponding oligothiophene 6-mer.[11d]

(30) The dication derived from unsubstituted *E,E*-**1** is by 4.05 kcal mol^{-1} more stable than the dication derived from unsubstituted *Z,Z*-**1** based on the calculation at the B3LYP/6-31G(d,p) level. Biradical character of the dication derived from unsubstituted *E,E*-**1** or *Z,Z*-**1** is 13.5% or 12.9%, respectively (Figure S28, Supporting Information).

(31) Kato, T.; Kikuchi, K.; Achiba, Y. *J. Phys. Chem.* **1993**, *97*, 10251−10253.

(32) The sulfur atoms of *E,E*-**1** in the Saturn-like complex *E,E*-**1**⊃C_{60} are located on the five- and six-membered rings of C_{60}, in contrast to

DOI: 10.1021/jacs.5b00291
J. Am. Chem. Soc. 2015, 137, 3877−3885

Kawase's [6]CPPA, in which all benzene rings lie over the 5:6 ring fusion of C_{60}.[3a]
(33) The amorphous film of **2** and C_{60} (1:1) consists of the amorphous **2** and aggregated C_{60}[38] separately.
(34) Iyoda, M.; Huang, P.; Nishiuchi, T.; Takase, M.; Nishinaga, T. *Heterocycles* **2011**, *82*, 1143−1149.
(35) Kawase, T.; Darabi, H. R.; Uchiyama, R.; Oda, M. *Chem. Lett.* **1995**, *24*, 499−500.
(36) Iyoda, M.; Shimizu, H. *Chem. Soc. Rev.* in press.
(37) (a) Bond, A. M.; McLennan, E. A.; Stojanovic, R. S.; Thomas, F. G. *Anal. Chem.* **1987**, *59*, 2853−2860. (b) Trasalti, S. *Pure Appl. Chem.* **1986**, *58*, 956−966. (c) Cardona, C. M.; Li, W.; Kaifer, A. E.; Stockdale, D.; Bazan, G. C. *Adv. Mater.* **2011**, *23*, 2367−2371.
(38) (a) Ying, Q.; Marecek, J.; Chu, B. *Chem. Phys. Lett.* **1994**, *219*, 214−218. (b) Rudalevige, T.; Francis, A. H.; Zand, R. *J. Phys. Chem. A* **1998**, *102*, 9797−9802. (c) Chen, K. L.; Elimelech, M. *Langmuir* **2006**, *22*, 10994−11001.

DOI: 10.1021/jacs.5b00291
J. Am. Chem. Soc. 2015, 137, 3877−3885